


## EFFECT OF RARE EARTH METALS ON POROSITY FORMATION IN A356 ALLOY

M. G. Mahmoud, E. M. Elgallad, M. F. Ibrahim, and F. H. Samuel 

Département des sciences appliquées, Université du Québec à Chicoutimi, Chicoutimi, QC, Canada

Copyright © 2017 American Foundry Society  
DOI 10.1007/s40962-017-0156-5

### Abstract

*The present study was performed on A356 alloy containing various amounts of La, Ce or La + Ce, without and with about 80–100 ppm Sr. The main objective was to evaluate the porosity formed in rare earth metals (RE) containing Al–Si cast alloys. The results reveal that the addition of large amounts of RE (approximately 3%) would cause a marked increase in the freezing zone coupled with a marked volume fraction of RE-based intermetallics which would reduce the alloy feedability, leading to the formation of a significant percentage of shrinkage porosity. This*

*situation is more severe in Sr-treated alloys. The depression in the eutectic Si temperature is not necessarily a parameter to consider in determining the degree of eutectic modification. Cerium is relatively more effective than La in terms of porosity formation.*

**Keywords:** rare earth metals, shrinkage porosity, Al–Si alloys, solidification rate

### Introduction

A review article on the effects of casting quality, microstructure and mechanical properties of cast Al–Si–0.3 Mg alloy was presented by Nallusamy.<sup>1</sup> It is inferred from this review that rare earth (RE) elements such as La (Lanthanum), Ce (Cerium), Y (Yttrium), and MM (misch metal) are reported to act as effective eutectic silicon modifiers.<sup>2</sup> Based on experimental results, it was found that the addition of a minor amount of MM ( $\leq 0.2$  wt%) results in partial modification while higher MM additions (0.3–1.0 wt%) produce full modification. Misch metal addition increases under cooling up to 25 K (25 °C/45 °F) with 0.2% addition giving rise to modified precipitate shapes. It forms intermetallic compounds such as Al<sub>4</sub>Ce, Al<sub>4</sub>La, Al<sub>2</sub>Ce, SiCe, SiCe<sub>2</sub> that would suppress growth of Si.<sup>3–7</sup>

Studies on rare earths as micro-alloying elements revealed that these elements may have some beneficial effects on the mechanical properties of aluminum alloys.<sup>8,9</sup> It was reported that addition of Ce to Al–Cu–Mg–Ag alloy improved the thermal stability of the  $\Omega$  phase thus raising the service temperature of this alloy.<sup>10</sup> Fang et al.<sup>11</sup> demonstrated that adding 0.1–0.2% (mass fraction) Y improved the tensile properties of 2519 alloy at room and elevated temperatures as Y changing the size and density of the  $\theta'$  phase. It was indicated that Nd was mainly distributed in the form of an

intermediate compound AlCuNd, which exerted a restraining force on the grain boundaries and enhanced the mechanical properties of 2519 alloy at high temperature.<sup>12</sup> Some recent studies showed that Yb may be considered as an effective micro-alloying element in aluminum alloys. It was reported that Yb addition improved the mechanical properties of Al–Cu–Mg–Ag alloy and Al–Zn–Mg–Cu–Zr alloy.<sup>13</sup> According to Sigworth,<sup>14</sup> while a number of IA and IIA elements and several lanthanides produce a modified eutectic, only strontium and sodium have found significant commercial application.

Dahle et al.<sup>15</sup> reported on the role of eutectic growth mode in porosity formation in Al–Si alloys. Their results show that the formation of the eutectic may significantly affect the permeability of the mushy zone by preferentially forming in the interdendritic flow paths, or it may evolve from the surface toward the center and therefore with a much wider feed path. Porosity formation in aluminum alloy A356 modified with Ba, Ca, Y and Yb was studied by Knuutinen et al.<sup>16</sup> who found that additions of Ba and Yb resulted in small, round, dispersed porosity. When porosity formation is considered based on the feeding mechanisms, particularly interdendritic feeding, it is possible to rationalize the effects of the elements on porosity distribution based on their impact on the eutectic solidification mode.

**Table 1. Chemical Compositions of the Base A356 Alloy**

| Alloy | Elements (wt%) |      |      |     |     |     |
|-------|----------------|------|------|-----|-----|-----|
|       | Si             | Mn   | Mg   | Fe  | Zn  | Cr  |
| A356  | 7.2            | 0.20 | 0.35 | 0.2 | 0.1 | 0.1 |

In spite of the large number of publications on the effect of rare earth metals on the microstructure and mechanical properties of 356 alloy, almost no information is available on porosity formation in this category of alloys and hence the present study was undertaken to address this issue.

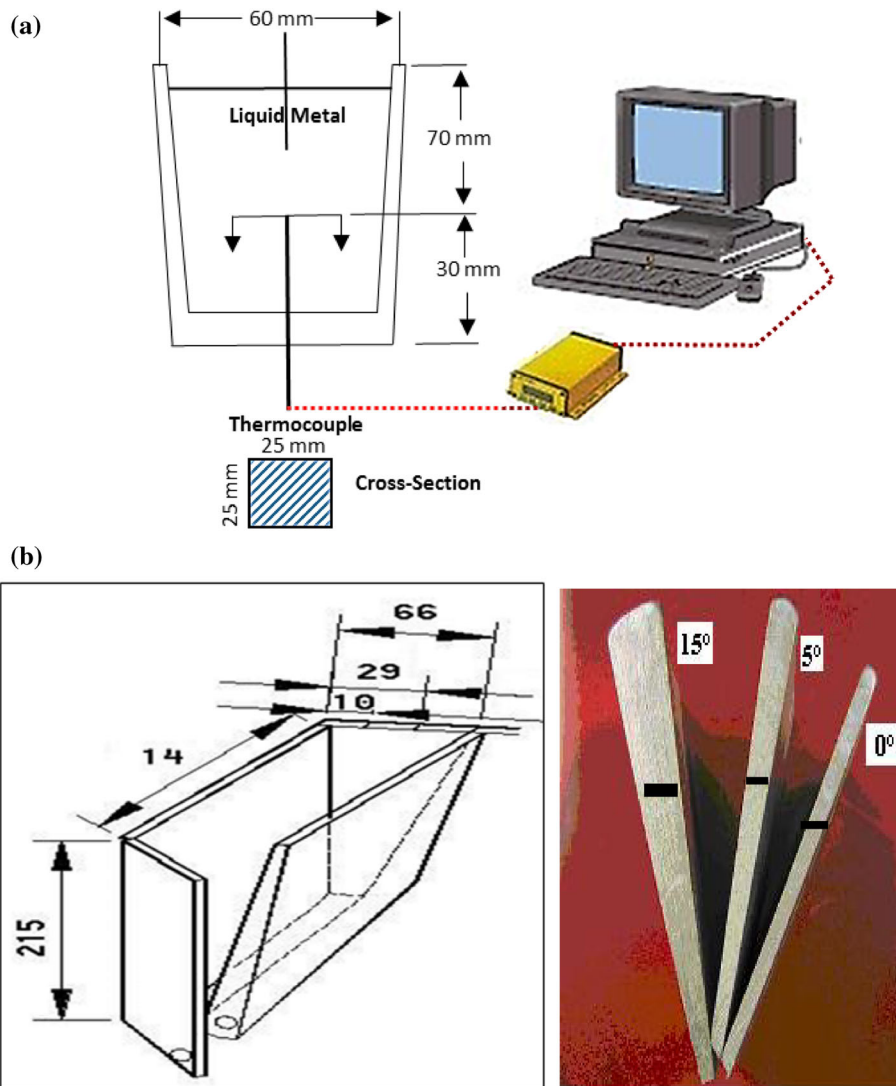
### Experimental Procedure

Table 1 lists the chemical composition of the base A356 alloy used in the present study. The as-received ingots were

melted using an electrical resistance furnace at 750 °C. The molten metal was degassed using a graphite rotary impeller at speed of 130 rpm. Prior to degassing using pure Ar for 20 min., measured amounts of Sr, La or Ce were added. The three elements were introduced into the molten alloy in the form of Al-10%Sr, Al-20%La and Al-20%Ce master alloys. It should be mentioned here that the non-modified casting was made first, followed by addition of Sr, degassing, then pouring the second half of the melt to produce the Sr-modified casting. In each case, at the end of the degassing period the molten alloy was poured in two different molds:

1. Graphite mold heated at 600 C for obtaining the solidification curve—Figure 1a.
2. Variable angle metallic mold (0°, 5°, 15°) heated at 350 °C—Figure 1b.

For each pouring/casting, samplings for chemical analysis were also taken, to determine the exact composition of the



**Figure 1. (a) Thermal analysis setup. (b) Variable metallic mold (left-dimensions are in mm) and castings (right)—black bands indicate positions of metallographic samples.**

melt. Five samples for chemical analysis were also taken simultaneously from each alloy during casting so as to make sure that the actual average chemical compositions were obtained. The chemical analysis was carried out using a Spectrolab Jr CCD Spark Analyzer at General Motors facilities in Warren, MI, and the results are listed in Tables 2 and 3. The microstructures were examined by means of a Leica DM LM optical microscope in conjunction with a Clemex image analyzer. The porosity size was obtained from the average of 200 measurements taken over 20 fields (10 measurements per field) at 100× magnification for each alloy sample. Porosity was also viewed using an electron probe microanalyzer (EPMA) in conjunction with energy-dispersive X-ray analysis (EDX) and wavelength-dispersive spectroscopic analysis (WDS) where

required, integrating a combined JEOL JXA-8900 1 WD/ED microanalyzer operating at 20 kV and 30 nA, where the size of the spot examined was ~2 μm. Table 4 lists the secondary dendrite arm spacing (SDAS) values measured, using line intercept methods.

## Results and Discussion

### Graphite Mold

Figure 2a shows the solidification curve obtained from the base A356 alloy in which the precipitation of α-Al starts at 611 °C and the eutectic (Al–Si) reaction takes place at 570 °C. According to Ferdian et al.,<sup>17</sup> the eutectic

**Table 2. Chemical Composition and Codes of the Actual Alloys—Graphite Mold**

| Alloy | Mold type | Mold temp (°C) | Alloy code | Modifier addition (wt%) |       |       |        |       |       |
|-------|-----------|----------------|------------|-------------------------|-------|-------|--------|-------|-------|
|       |           |                |            | Aimed                   |       |       | Actual |       |       |
|       |           |                |            | Sr                      | La    | Ce    | Sr     | La    | Ce    |
| 356   | Graphite  | 600            | TB         | 0                       | 0     | 0     | 0      | 0     | 0     |
|       |           |                | T10        | 0                       | 0.2   | 0     | 0      | 0.165 | 0     |
|       |           |                | T1         | 0                       | 0.5   | 0     | 0      | 0.356 | 0     |
|       |           |                | T2         | 0                       | 1     | 0     | 0      | 0.885 | 0     |
|       |           |                | T3         | 0                       | 1.5   | 0     | 0      | 1.225 | 0     |
|       |           |                | T11        | 0                       | 0     | 0.2   | 0      | 0.032 | 0.082 |
|       |           |                | T4         | 0                       | 0     | 0.5   | 0      | 0.136 | 0.185 |
|       |           |                | T5         | 0                       | 0     | 1     | 0      | 0.046 | 0.817 |
|       |           |                | T6         | 0                       | 0     | 1.5   | 0      | 0.089 | 1.088 |
|       |           |                | T7         | 0                       | 0.5   | 0.5   | 0      | 0.44  | 0.282 |
|       |           |                | T8         | 0                       | 1     | 1     | 0      | 0.781 | 0.777 |
|       |           |                | T9         | 0                       | 1.5   | 1.5   | 0      | 1.073 | 0.931 |
|       |           |                | TBS        | 0.01                    | 00    | 00    | 0.0071 | 00    | 00    |
|       |           |                | T10S       | 0.01                    | 0.2   | 0     | 0.0069 | 0.165 | 0     |
|       |           |                | T1S        | 0.01                    | 0.5   | 0     | 0.0109 | 0.356 | 0     |
|       |           |                | T2S        | 0.01                    | 1     | 0     | 0.0047 | 0.685 | 0     |
|       |           |                | T3S        | 0.01                    | 1.5   | 0     | 0.0047 | 1.025 | 0     |
|       |           |                | T11S       | 0.01                    | 0     | 0.2   | 0.0073 | 0.032 | 0.082 |
|       |           |                | T4S        | 0.01                    | 0     | 0.5   | 0.0075 | 0.136 | 0.185 |
|       |           |                | T5S        | 0.01                    | 0     | 1     | 0.0061 | 0.046 | 0.317 |
| T6S   | 0.01      | 0              | 1.5        | 0.0072                  | 0.089 | 1.088 |        |       |       |
| T7S   | 0.01      | 0.5            | 0.5        | 0.0068                  | 0.44  | 0.282 |        |       |       |
| T8S   | 0.01      | 1              | 1          | 0.0073                  | 0.781 | 0.877 |        |       |       |
| T9S   | 0.01      | 1.5            | 1.5        | 0.0066                  | 1.073 | 0.931 |        |       |       |

All castings contain 0.05% Ti

**Table 3. Chemical Composition and Codes of the Actual Alloys—Variable Angle Mold**

| Alloy | Mold type            | Mold temp (°C) | Alloy code | Modifier addition (wt%) |       |        |        |       |       |
|-------|----------------------|----------------|------------|-------------------------|-------|--------|--------|-------|-------|
|       |                      |                |            | Aimed                   |       |        | Actual |       |       |
|       |                      |                |            | Sr                      | La    | Ce     | Sr     | La    | Ce    |
| A356  | Variable angle (15°) | 350            | DBL        | 0                       | 0     | 0      | 0      | 0     | 0     |
|       |                      |                | D10L       | 0                       | 0.2   | 0      | 0      | 0.165 | 0     |
|       |                      |                | D1L        | 0                       | 0.5   | 0      | 0      | 0.356 | 0     |
|       |                      |                | D2L        | 0                       | 1     | 0      | 0      | 0.685 | 0     |
|       |                      |                | D3L        | 0                       | 1.5   | 0      | 0      | 1.025 | 0     |
|       |                      |                | D11L       | 0                       | 0     | 0.2    | 0      | 0.032 | 0.082 |
|       |                      |                | D4L        | 0                       | 0     | 0.5    | 0      | 0.136 | 0.185 |
|       |                      |                | D5L        | 0                       | 0     | 1      | 0      | 0.046 | 0.317 |
|       |                      |                | D6L        | 0                       | 0     | 1.5    | 0      | 0.089 | 1.088 |
|       |                      |                | D7L        | 0                       | 0.5   | 0.5    | 0      | 0.44  | 0.282 |
|       | D8L                  | 0              | 1          | 1                       | 0     | 0.781  | 0.877  |       |       |
|       | D9L                  | 0              | 1.5        | 1.5                     | 0     | 1.073  | 0.931  |       |       |
|       | Variable angle (15°) | 350            | DBLS       | 0.01                    | 0     | 0      | 0.0120 | 0     | 0     |
|       |                      |                | D10LS      | 0.01                    | 0.2   | 0      | 0.0069 | 0.165 | 0     |
|       |                      |                | D1LS       | 0.01                    | 0.5   | 0      | 0.0109 | 0.356 | 0     |
|       |                      |                | D2LS       | 0.01                    | 1     | 0      | 0.0077 | 0.685 | 0     |
|       |                      |                | D3LS       | 0.01                    | 1.5   | 0      | 0.0077 | 1.025 | 0     |
|       |                      |                | D11LS      | 0.01                    | 0     | 0.2    | 0.0073 | 0.033 | 0.082 |
|       |                      |                | D4LS       | 0.01                    | 0     | 0.5    | 0.0072 | 0.136 | 0.385 |
|       |                      |                | D5LS       | 0.01                    | 0     | 1      | 0.0071 | 0.046 | 0.817 |
| D6LS  |                      |                | 0.01       | 0                       | 1.5   | 0.0078 | 0.089  | 1.088 |       |
| D8LS  |                      |                | 0.01       | 1                       | 1     | 0.0075 | 0.781  | 0.877 |       |
| D9LS  | 0.01                 | 1.5            | 1.5        | 0.0078                  | 1.073 | 0.931  |        |       |       |

All castings contain 0.05% Ti

**Table 4. Average Dendrite Arm Spacings of A356 Alloy Samples**

| Mold           | Mold temperature (°C) | Mold section | SDAS <sup>a</sup> (μm) |       |
|----------------|-----------------------|--------------|------------------------|-------|
|                |                       |              | Average                | S. D. |
| Graphite       | 600                   | Center       | 86.63                  | 12.49 |
| Variable angle | 350                   | Large        | 52.62                  | 5.7   |
|                | 350                   | Medium       | 39.5                   | 4.8   |
|                | 350                   | Small        | 21.04                  | 3.6   |

<sup>a</sup> Secondary dendrite arm spacing obtained over 20 measurements taken from each sample

S. D.: standard deviation

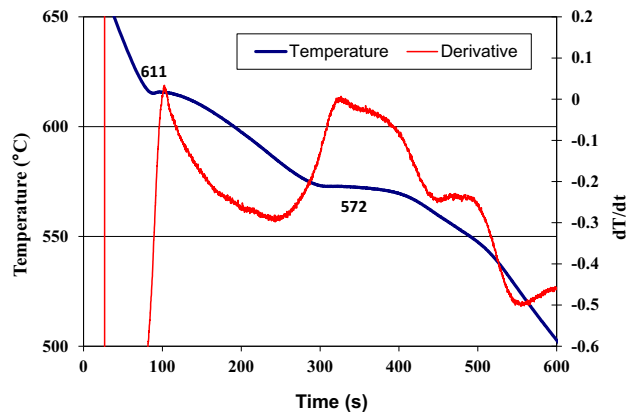
temperature of a given alloy can be determined by Eqn. (1). Thus, for the present alloy  $T_R$  should be close to 572 °C. In the present, the calculated  $T_R$  is approximately 572.5 °C corresponding to the eutectic temperature in the

present case, which is very close to the calculated temperature. Addition of 1.5%Ce +1.5%La (alloy coded T9, Table 2) resulted in increasing the  $\alpha$ -Al precipitation temperature to 621 °C, with a major decrease in the eutectic temperature to 559 °C leading to an increase in the freezing zone by about 22 °C. It is also inferred from Figure 2b that there are two peaks in the mushy zone due to precipitation of La-, Ce-rich phases, 594 and 580 °C, respectively—Figure 2c–f. It is well established that the depression in the eutectic temperature could be used as an indicator of eutectic Si modification.<sup>14</sup>

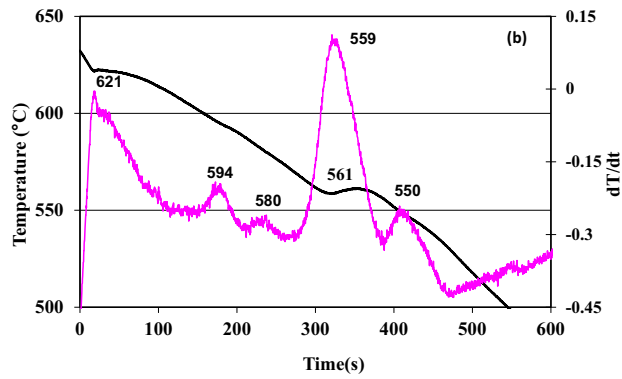
$$T_R(°C) = 577 - \frac{12.5}{w_{Si}} \cdot (4.59) \cdot w_{Mg} + 1.37 \cdot w_{Fe} + 1.65 \cdot w_{Cu} + 0.35 \cdot w_{Zn} + 2.54 \cdot w_{Mn} + 3.52 \cdot w_{Ni}$$

Eqn. 1

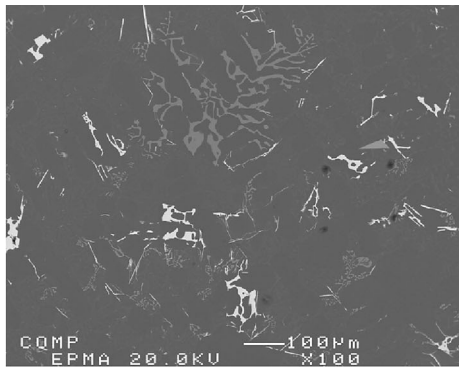
Figure 3a presents the solidification curve of the base A356 alloy modified with about 71 ppm Sr (coded TBS) where the eutectic temperature is approximately 565 °C, which is



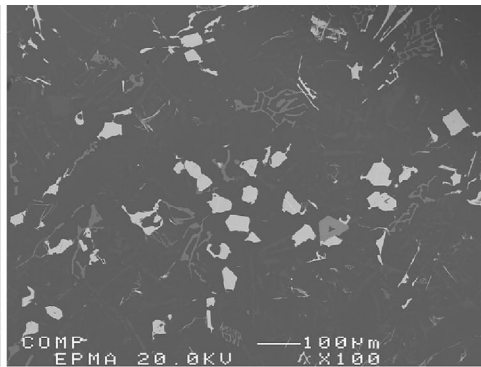
(a)



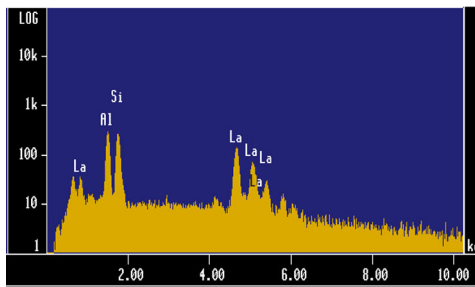
(b)



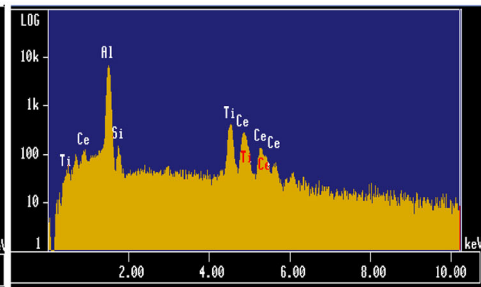
(c)



(d)



(e)



(f)

**Figure 2. Solidification curves and their first derivatives obtained from non-modified A356 alloy: (a) as received, (b) as-received A356 alloy + 1.5%La + 1.5%Ce, (c) La-rich phase, (d) Ce-rich phase, (e) EDS spectrum corresponding to (c), (f) EDS spectrum corresponding to (d)—as-received A356 alloy + 1.5%La + 1.5%Ce.**

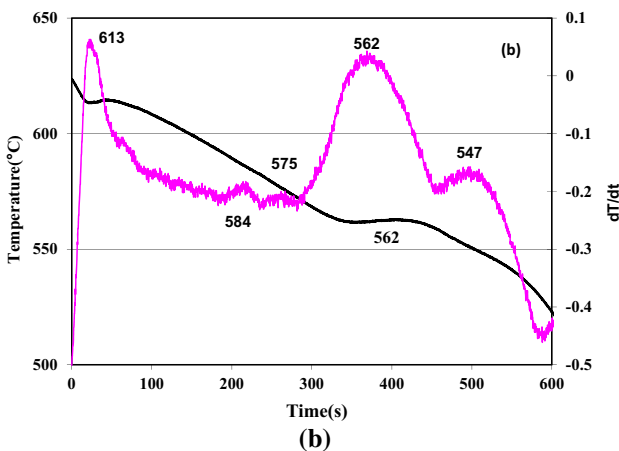
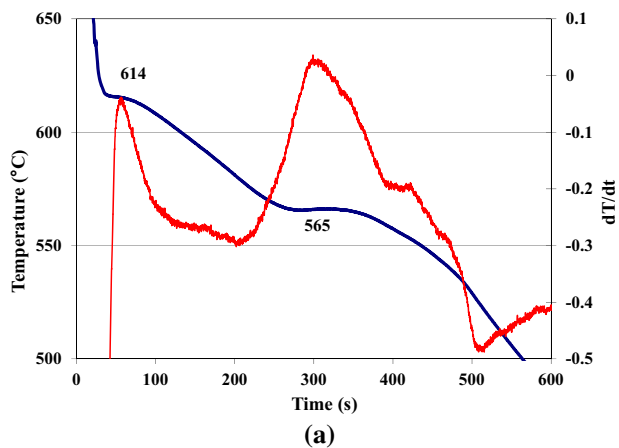


**Figure 3. Solidification curves and their first derivatives obtained from Sr-modified A356 alloy: (a) as received, (b) as-received A356 alloy + 1.5%La + 1.5%Ce.**

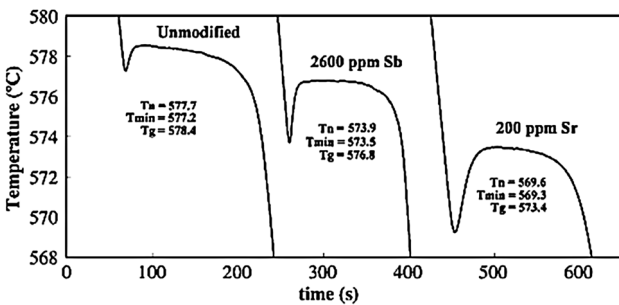


**Figure 4. Comparison of cooling curves from unmodified, Sb-modified (2600 ppm) and Sr-modified (200 ppm), Al-10% Si samples. The nucleation temperature ( $T_n$ ), minimum temperature prior to recalescence ( $T_{min}$ ) and the growth temperature ( $T_g$ ) are included in the figure.<sup>21</sup>**

about 7 °C lower than that in Figure 2b.<sup>17–20</sup> Addition of La and Ce to the Sr-modified alloy (coded T9S) produced more or less same features shown in Figure 2a, as shown in Figure 3b with a slight decrease in the eutectic temperature, i.e., 562 °C.

Dahle et al.<sup>21</sup> investigated eutectic modification and microstructure development in Al–Si alloys. Their results show that antimony additions resulted in a depression of the eutectic nucleation and growth temperatures and an increase in the amount of recalescence prior to growth. Similar but larger effects were observed with strontium modification. Figure 4 illustrates typical cooling curves in the vicinity of the eutectic reaction for the alloys used in their research.

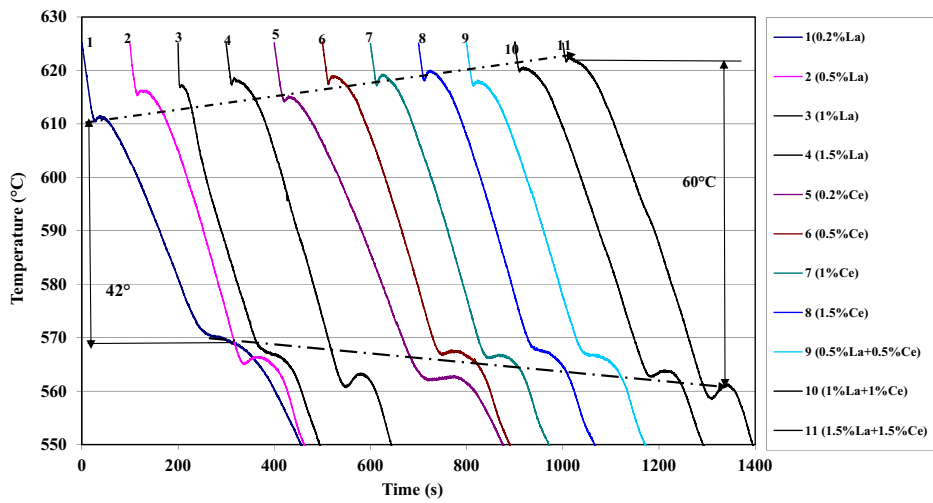
Figure 5a shows the successive variations in both  $\alpha$ -Al and (Al–Si) eutectic temperatures with the increase in the added amount of rare earth metals. These variations diminished significantly when the alloys were modified with Sr—Figure 5b. Ahmad and Asmael<sup>22</sup> analyzed the influence of La on solidification, microstructure, and mechanical properties of eutectic Al-11%Si- piston alloy. The cooling curve and microstructure analysis showed that La altered the Si structure. The nucleation and growth temperatures of eutectic Si decreased when 0.3 wt% La was added, and a high depression temperature was obtained with 1.0 wt% La as shown in Figure 5a–c. The thermal analysis result recorded a faster freezing time with the La addition and a 36% alteration in the secondary dendrite arm spacing. In contrast to the published data on the modification effect of addition of large amounts of La or Ce, Figure 6 reveals partial modification following the addition of 1.5%La—no Sr was added. Examples of porosity in (La + Ce) containing alloys are shown in Figure 7 revealing the presence of rare earth-rich phases inside the pores.

### Variable Angle Mold

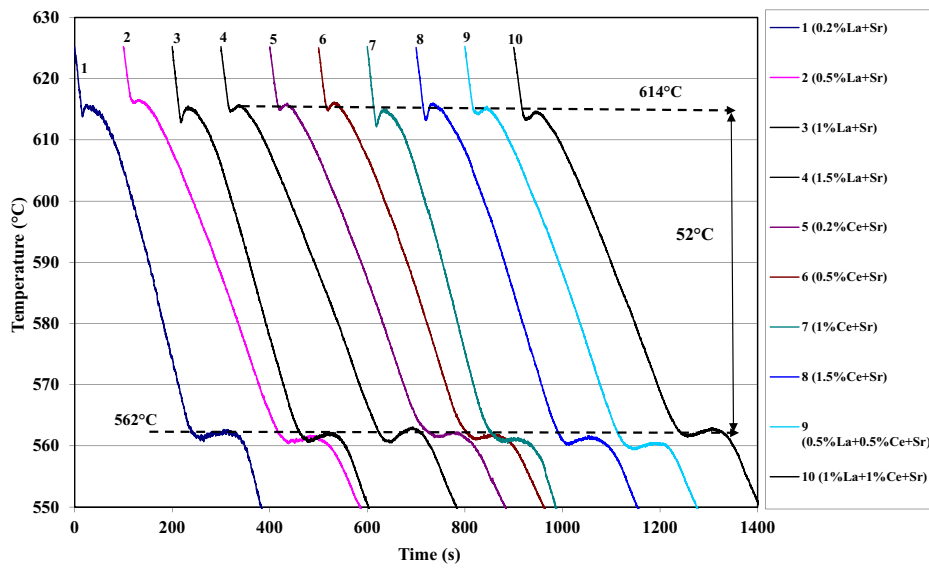
Figure 8 displays radiographs obtained from sections prepared from the three positions of the mold, before and after degassing. These radiographs show the effectiveness of degassing in minimizing porosity in the base alloy. Porosity characteristics obtained from small- and large-angle castings are listed in Tables 5, 6, 7 and 8. It should be noted that the same melt was poured for preparing both large- and small-angle castings. In the latter case, the sample codes were suffixed with an ‘S’. For Sr-modified melts, a second ‘S’ was added at the end in the sample code.

It is evident from these tables that:

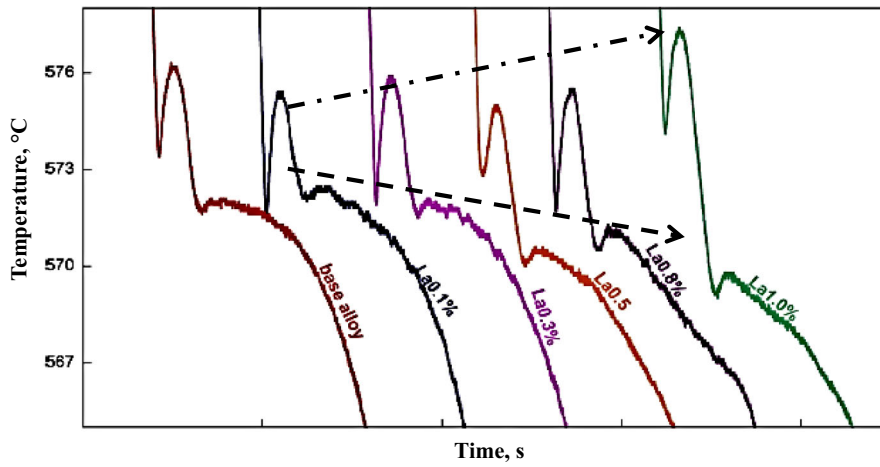
1. Measurements made from small sections may be affected by scattered hot spots. However, in general both average pore area and length increase with the increase in the amount of added rare earth (RE) metals. Combined addition of Sr and RE has a marginal effect on the pore characteristics.



(a)



(b)



(c)

**Figure 5. (a) Temperature–time curves of A356 alloy with various amounts of La and Ce. (b) Temperature–time curves of Sr-modified A356 alloy with various amounts of La and Ce. (c) Solidification curves of Al-11Si-Cu-Mg alloy with and without La addition.<sup>22</sup>**

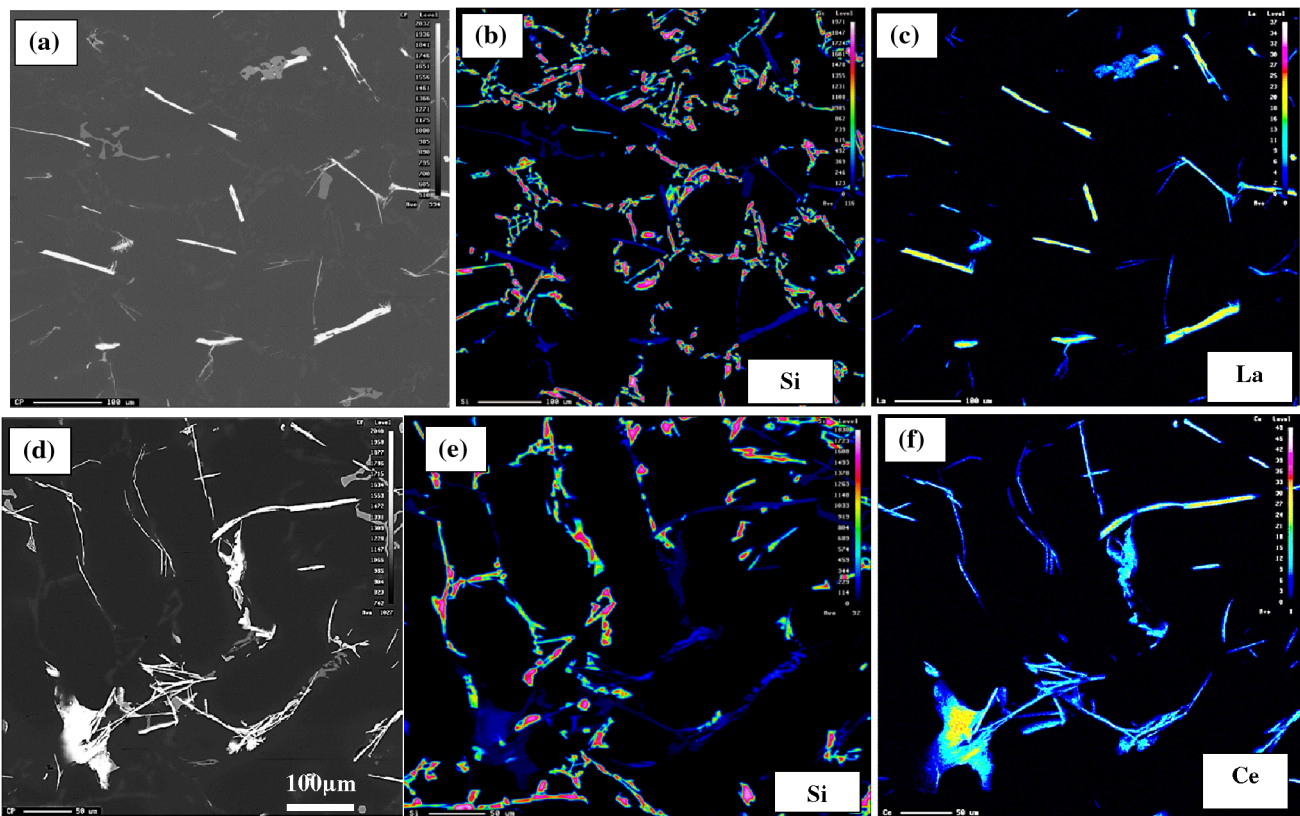
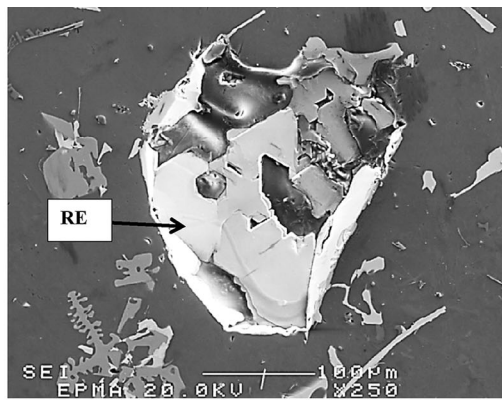


Figure 6. Eutectic Si size and distribution in La and Ce containing alloys: (a–c) T3 alloy, (d–f) T6 alloy.

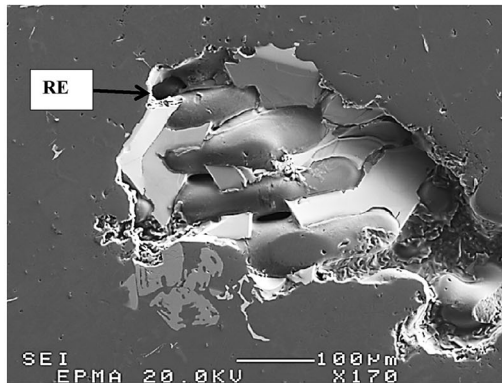
2. Increasing the freezing zone caused by the increase in the added amount of RE (Figure 5) is expected to result in enhancing porosity formation.<sup>23,24</sup> According to Samavedam and Sundarajan,<sup>23</sup> chills promote steeper temperature gradients in the solidifying metal and increase its feeding capacity, thereby reducing shrinkage. Also, a number of pores originate from the mold filling stage and entrainment of oxide films, while others appear due to insufficient feeding during solidification.<sup>24</sup>
3. Another parameter to be considered is the presence of a large volume fraction of intermetallics in the form of platelets (Figures 6 and 7) which would hinder the metal feeding ability similar to that reported for  $\beta$ -Al<sub>3</sub>FeSi phase.<sup>25–29</sup>

One of the most important aspects of the quality of an alloy casting is the presence or absence of porosity in the casting. Porosity occurs in solidifying metals and alloys due to negative pressures generated during solidification contraction, and pressure developed by gases dissolved in the molten metal. Both these processes may act either together or separately to produce shrinkage or gas defects. They are generally unwanted and constitute a major problem.<sup>30</sup> Porosity formation is essentially a nucleation and growth process involving heterogeneous nucleation in the early stages of solidification due to entrapped inclusions and contact with the mold wall or existing gas bubbles. The possibility of homogenous nucleation also exists, especially in the later stages of solidification in the interdendritic regions of the mushy zone, a zone defined by the freezing range of the alloy, where the presence of entrapped nuclei is less likely to occur.<sup>31</sup>

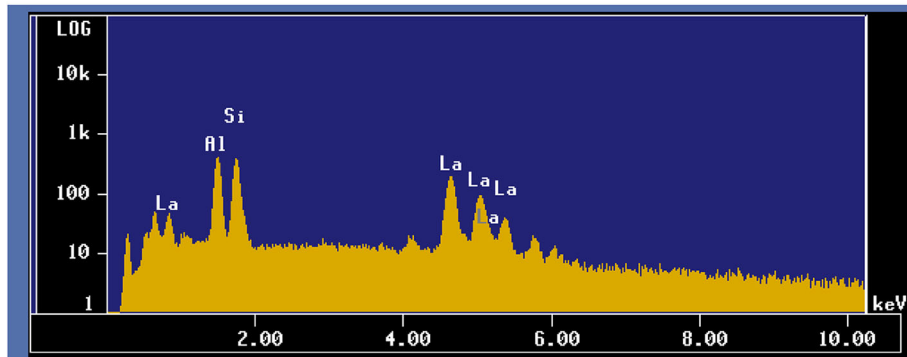




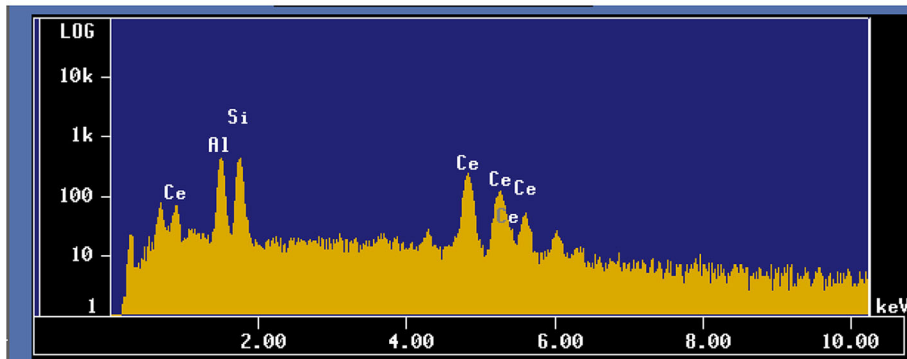
(a)



(b)



(c)



(d)

**Figure 7. Examples of porosity formed in A356 alloy containing high levels of La + Ce:(a) T9 alloy, plate-like intermetallic, (b) T9S alloy, branched intermetallic, (c) EDS spectrum corresponding to (a) revealing reflections due to La, (d) EDS spectrum corresponding to (b) revealing reflections due to Ce.**

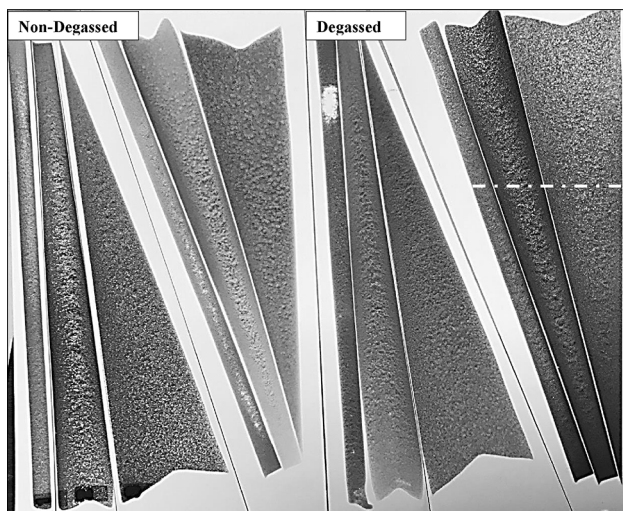


**Figure 8. Radiographs of sections from the variable mold—white line indicating the position of metallographic samples.**

**Table 5. Porosity Characteristics of Non-modified A356 Alloy—Variable Angle Mold (small)**

| Alloy code | Pore characteristics     |       |                          |       |                                  |
|------------|--------------------------|-------|--------------------------|-------|----------------------------------|
|            | Area ( $\mu\text{m}^2$ ) |       | Length ( $\mu\text{m}$ ) |       | Density (#pores/ $\text{mm}^2$ ) |
|            | Average                  | S. D. | Average                  | S. D. |                                  |
| DBS        | 125.1                    | 63.1  | 28.5                     | 2.8   | 125                              |
| D10S       | 348.3                    | 22.9  | 13.5                     | 3.3   | 152                              |
| D1S        | 148.4                    | 75.5  | 33.9                     | 5.4   | 179                              |
| D2S        | 166.4                    | 70.2  | 32.1                     | 6.9   | 175                              |
| D3S        | 367.3                    | 54.2  | 60.3                     | 4.6   | 240                              |
| D11S       | 347.5                    | 37.2  | 48.7                     | 24.9  | 111                              |
| D4S        | 651.6                    | 66.7  | 48.1                     | 31.8  | 140                              |
| D5S        | 139.2                    | 64.5  | 39.6                     | 26.6  | 180                              |
| D6S        | 527.9                    | 47.1  | 28.0                     | 23.2  | 210                              |
| D7S        | 217.5                    | 77.6  | 11.7                     | 17.1  | 250                              |
| D8S        | 286.6                    | 82.5  | 47.4                     | 22    | 175                              |
| D9S        | 562.9                    | 11.3  | 53.3                     | 6.1   | 240                              |

Mold temperature: 350 °C

Small: angle of variable angle mold is 0°

S. D.: standard deviation

**Table 6. Porosity Characteristics of Non-modified A356 Alloy—Variable Angle Mold (large)**

| Alloy code | Pore characteristics     |       |                          |       |                                  |
|------------|--------------------------|-------|--------------------------|-------|----------------------------------|
|            | Area ( $\mu\text{m}^2$ ) |       | Length ( $\mu\text{m}$ ) |       | Density (#pores/ $\text{mm}^2$ ) |
|            | Average                  | S. D. | Average                  | S. D. |                                  |
| DBL        | 152.5                    | 13.1  | 16.2                     | 7.1   | 181                              |
| D10L       | 119.4                    | 18.2  | 22.3                     | 8.2   | 62                               |
| D1L        | 506.1                    | 16.0  | 16.0                     | 6.0   | 352                              |
| D2L        | 320.4                    | 11.6  | 18.9                     | 1.6   | 229                              |
| D3L        | 929.8                    | 21.4  | 28.2                     | 11.4  | 254                              |
| D11L       | 833.0                    | 21.4  | 30.5                     | 12.4  | 258                              |
| D4L        | 927.1                    | 34.8  | 34.8                     | 9.8   | 285                              |
| D5L        | 590.6                    | 10.7  | 16.4                     | 7.7   | 320                              |
| D6L        | 455.8                    | 24.7  | 18.2                     | 5.7   | 357                              |
| D7L        | 104.7                    | 16.7  | 28.6                     | 6.7   | 260                              |
| D8L        | 355.7                    | 16.3  | 38.2                     | 6.3   | 330                              |
| D9L        | 721.0                    | 33.8  | 54.5                     | 12.8  | 400                              |

Mold temperature: 350 °C

Large: Angle of variable angle mold is 15°

S. D.: Standard deviation

**Table 7. Porosity Characteristics of Sr-Modified A356 alloy—Variable Angle Mold (small)**

| Alloy code | Pore characteristics     |       |                          |       |                                  |
|------------|--------------------------|-------|--------------------------|-------|----------------------------------|
|            | Area ( $\mu\text{m}^2$ ) |       | Length ( $\mu\text{m}$ ) |       | Density (#pores/ $\text{mm}^2$ ) |
|            | Average                  | S. D. | Average                  | S. D. |                                  |
| DBSS       | 260.2                    | 12.5  | 13.3                     | 8.5   | 162                              |
| D10SS      | 271.0                    | 19.4  | 17.5                     | 3.5   | 152                              |
| D1SS       | 516.2                    | 16.1  | 16.7                     | 3.9   | 179                              |
| D2SS       | 174.7                    | 20.4  | 13.2                     | 3.1   | 75                               |
| D3SS       | 123.1                    | 29.8  | 10.2                     | 6.3   | 240                              |
| D11SS      | 84.3                     | 33.0  | 10.2                     | 8.7   | 275                              |
| D4SS       | 244.6                    | 27.1  | 18.8                     | 8.1   | 222                              |
| D5SS       | 343.0                    | 90.6  | 16.4                     | 9.6   | 155                              |
| D6SS       | 343.2                    | 55.8  | 8.1                      | 8.0   | 184                              |
| D7SS       | 287.0                    | 14.7  | 19.5                     | 11.7  | 81                               |
| D8SS       | 382.8                    | 55.7  | 11.2                     | 7.4   | 163                              |
| D9SS       | 653.1                    | 62.9  | 27.1                     | 18.3  | 410                              |

Mold temperature: 350 °C

Small: Angle of variable angle mold is 0°

S. D.: Standard deviation

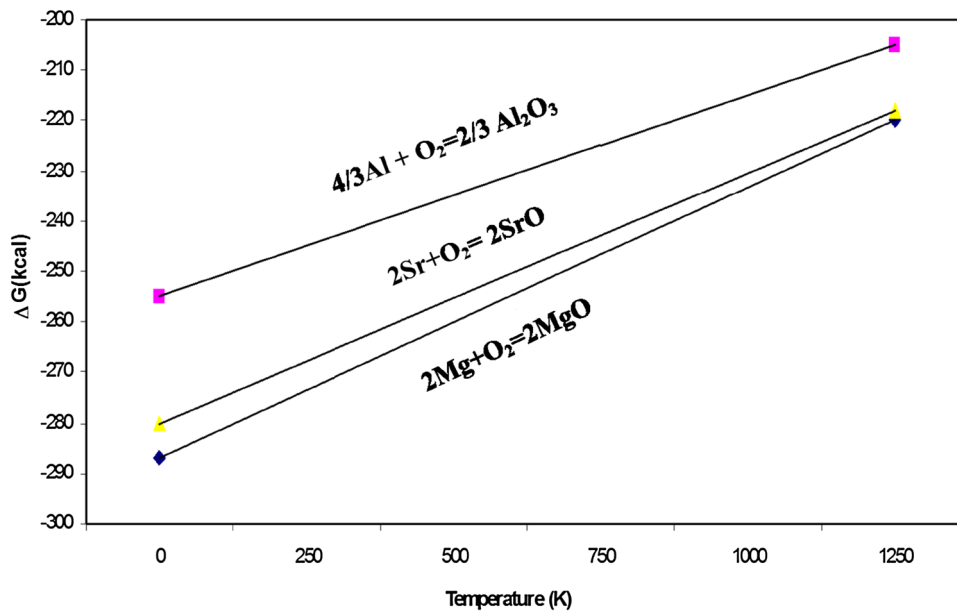


Figure 9. Free energy formation versus temperature for Al, Sr, and Mg oxides.<sup>27</sup>

Table 8. Porosity Characteristics of Sr-Modified A356—Variable Angle Mold (large)

| Alloy code | Pore characteristics     |       |                          |       |                                  |
|------------|--------------------------|-------|--------------------------|-------|----------------------------------|
|            | Area ( $\mu\text{m}^2$ ) |       | Length ( $\mu\text{m}$ ) |       | Density (#pores/ $\text{mm}^2$ ) |
|            | Average                  | S. D. | Average                  | S. D. |                                  |
| DBLS       | 282.0                    | 32.2  | 18.5                     | 7.8   | 155                              |
| D10LS      | 328.4                    | 24.7  | 13.5                     | 2.5   | 468                              |
| D1LS       | 669.6                    | 23.1  | 33.9                     | 3.8   | 652                              |
| D2LS       | 825.7                    | 64.3  | 32.1                     | 2.5   | 575                              |
| D3LS       | 1035.0                   | 104.6 | 60.3                     | 5.6   | 637                              |
| D11LS      | 878.1                    | 63.0  | 28.7                     | 8.4   | 249                              |
| D4LS       | 378.9                    | 43.2  | 48.1                     | 4.7   | 322                              |
| D5LS       | 653.6                    | 87.0  | 21.6                     | 5.0   | 474                              |
| D6LS       | 1188.5                   | 82.8  | 28.0                     | 2.4   | 342                              |
| D7LS       | 557.7                    | 53.1  | 31.7                     | 5.6   | 476                              |
| D8LS       | 1163.1                   | 76.2  | 47.4                     | 2.2   | 550                              |
| D9LS       | 1267.8                   | 96.7  | 58.3                     | 6.4   | 778                              |

Mold temperature: 350 °C

Large: angle of variable angle mold is 15°

S. D.: standard deviation

In the Sr-modified alloys, pores are often associated with the presence of strontium oxides. These SrO films or particles are formed due to the high oxygen affinity of strontium and are extremely difficult to be removed during degassing. As Figure 9 shows, the free energy of formation

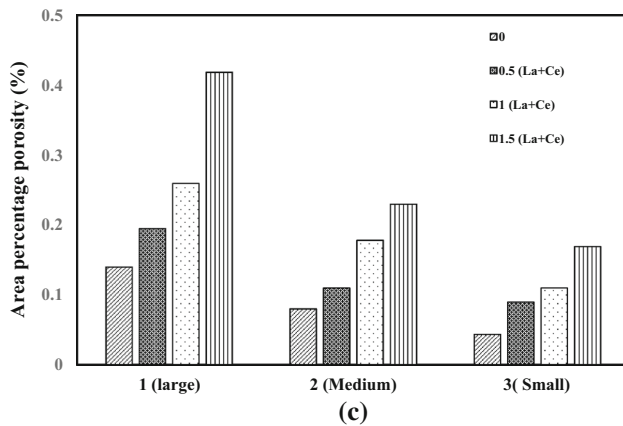
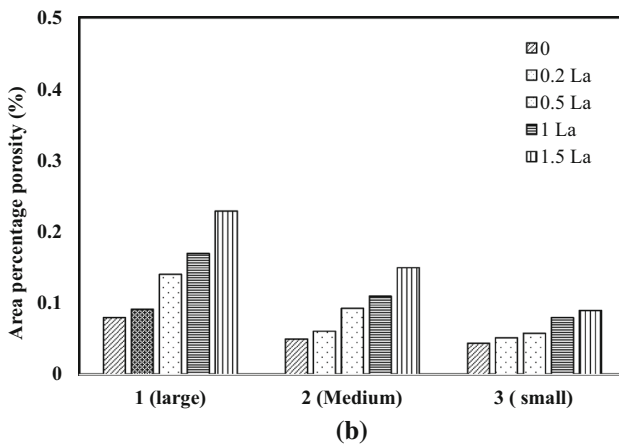
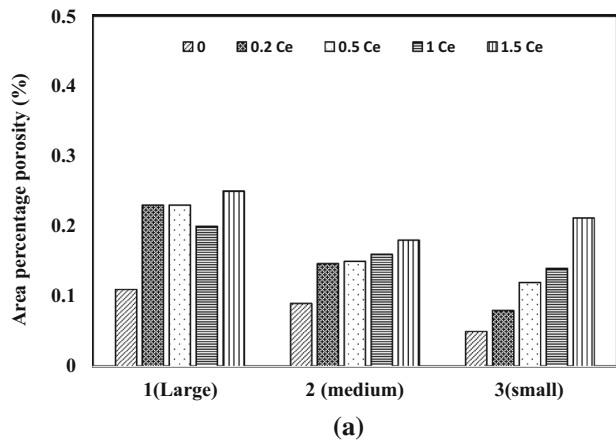
for SrO is lower than  $\text{Al}_2\text{O}_3$ . Thus, once formed, SrO is more stable than  $\text{Al}_2\text{O}_3$  and has a greater role in porosity formation. Also, the depression of the eutectic temperature with Sr addition can affect the eutectic solidification, leading to an extension of the freezing range of the alloy and an increase in the solidification time. Strontium also lowers the surface tension of the melt. Thus, it is expected that Sr-modified alloys will contain more porosity than the unmodified alloys.<sup>27</sup>

Figure 10 exhibits the combined effect of solidification rate and the concentration of RE on area porosity percentage in non-modified A356 alloy. From Figure 10a, b, it is evident that:

1. Cerium addition results in the formation of more porosity than La, especially at low solidification rate, and
2. The porosity percentage is directly related to the concentration of RE in the liquid metal.

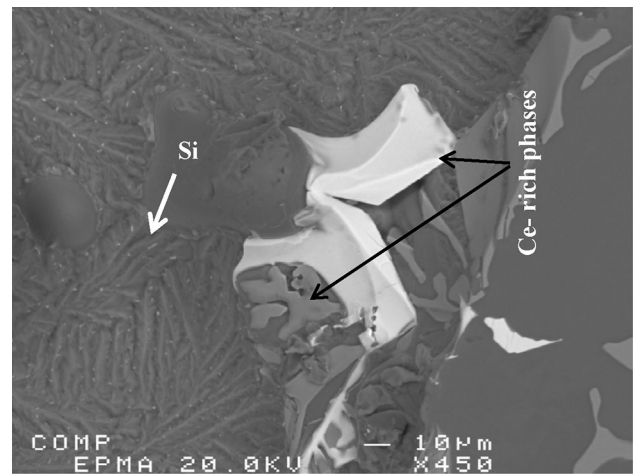
Figure 10c shows an explicit increase in porosity percentage when both Ce and La were added simultaneously to the liquid metal. Since the alloys were well degassed before pouring, the porosity should mostly be due to shrinkage. An example of the effect of Ce-rich phase (D9L alloy) on porosity formation in the large section-note the Si morphology is shown in Figure 11.

Figure 12 displays how the porosity density (measured by the number of pores/square mm) has been affected by the



**Figure 10. Variation in percentage of porosity as a function of solidification rate and amount of added RE: (a) Ce, (b) La, (c) La + Ce addition.**

solidification parameters and the concentration of RE. Examples of the microstructure of Sr-modified 356 alloy with different amounts of RE are shown in Figure 13. As



**Figure 11. Example of the effect of Ce-rich phase (D9L alloy) on porosity formation in the large section—note the Si morphology.**

expected most of the porosity is shrinkage type associated occasionally with oxide films (black arrow in Figure 13d). Figure 14 shows an example of the presence of SrO within pores in the D9LS sample obtained under reduced pressure test conditions.

## Conclusions

The present study was carried out with the main objective of evaluating the porosity in rare earth metals (RE) containing Al–Si cast alloys. The results reveal that:

1. The addition of large amounts of RE ( $\sim 3\%$ ) cause a marked increase in the freezing zone coupled with a marked volume fraction of RE-based intermetallics which would reduce the alloy feedability, leading to the formation of a significant percentage of shrinkage porosity.
2. The porosity formation is more severe in Sr-treated alloys since a part of the porosity may be associated with Sr-oxide films.
3. The depression in the eutectic Si temperature is not necessarily a parameter to consider in determining the degree of eutectic modification.
4. Cerium relatively promotes more porosity formation than La.

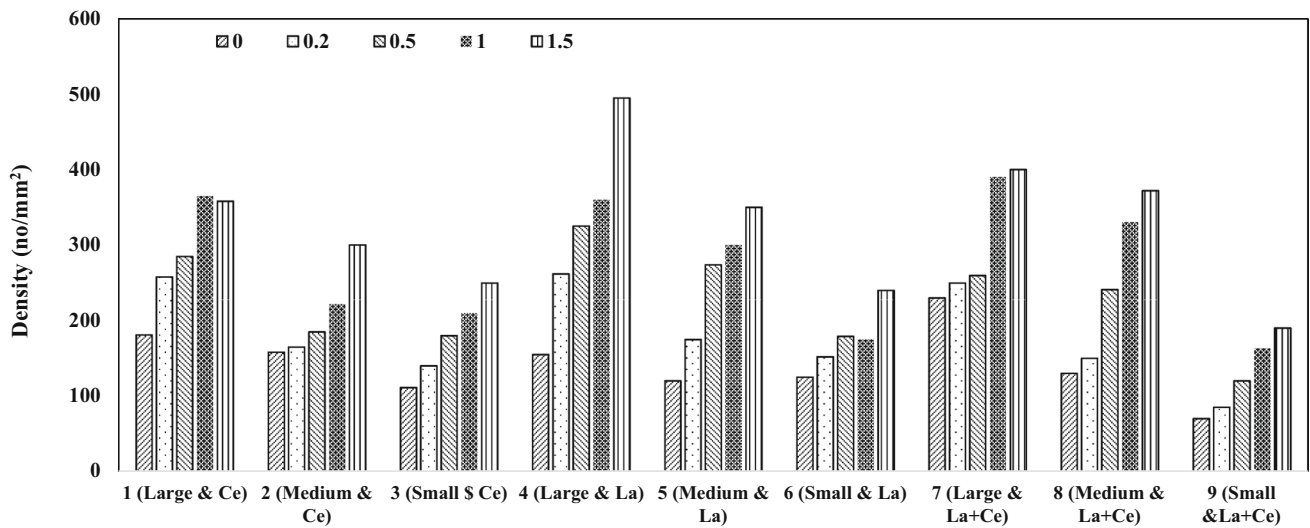


Figure 12. Variation in the density of porosity as a function of solidification rate and amount of added RE—see Table 5, 6, 7, 8 for actual La and Ce concentrations.

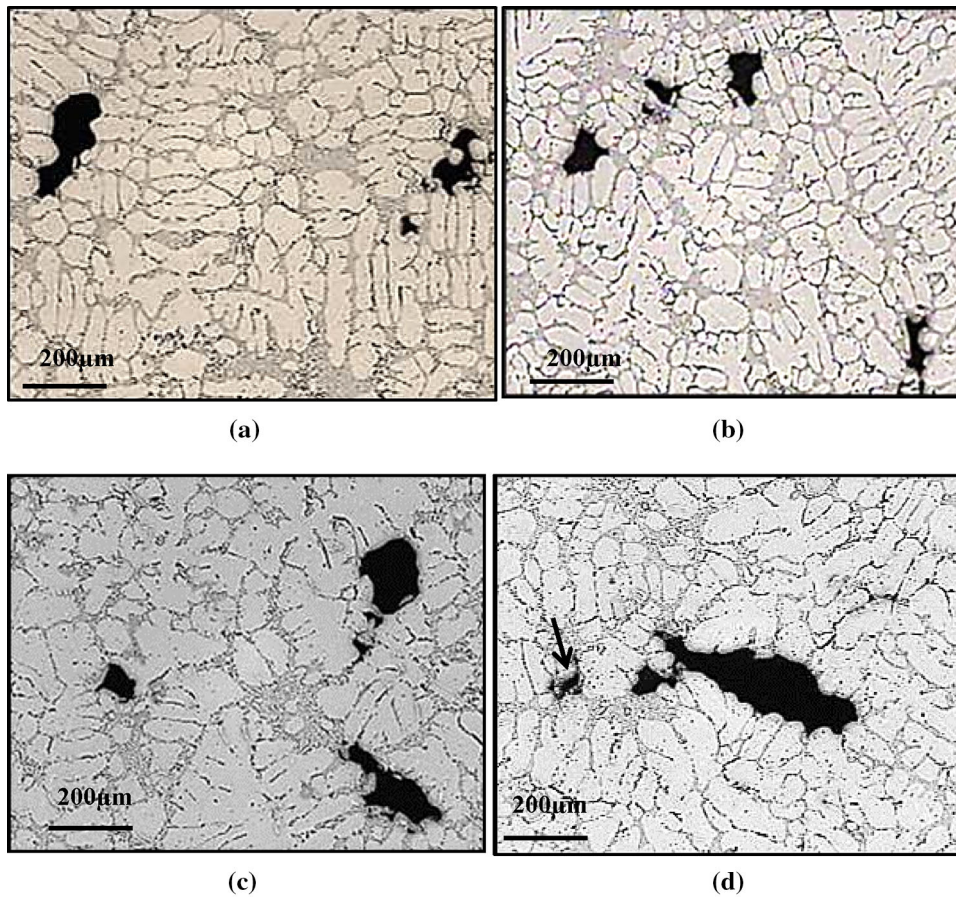
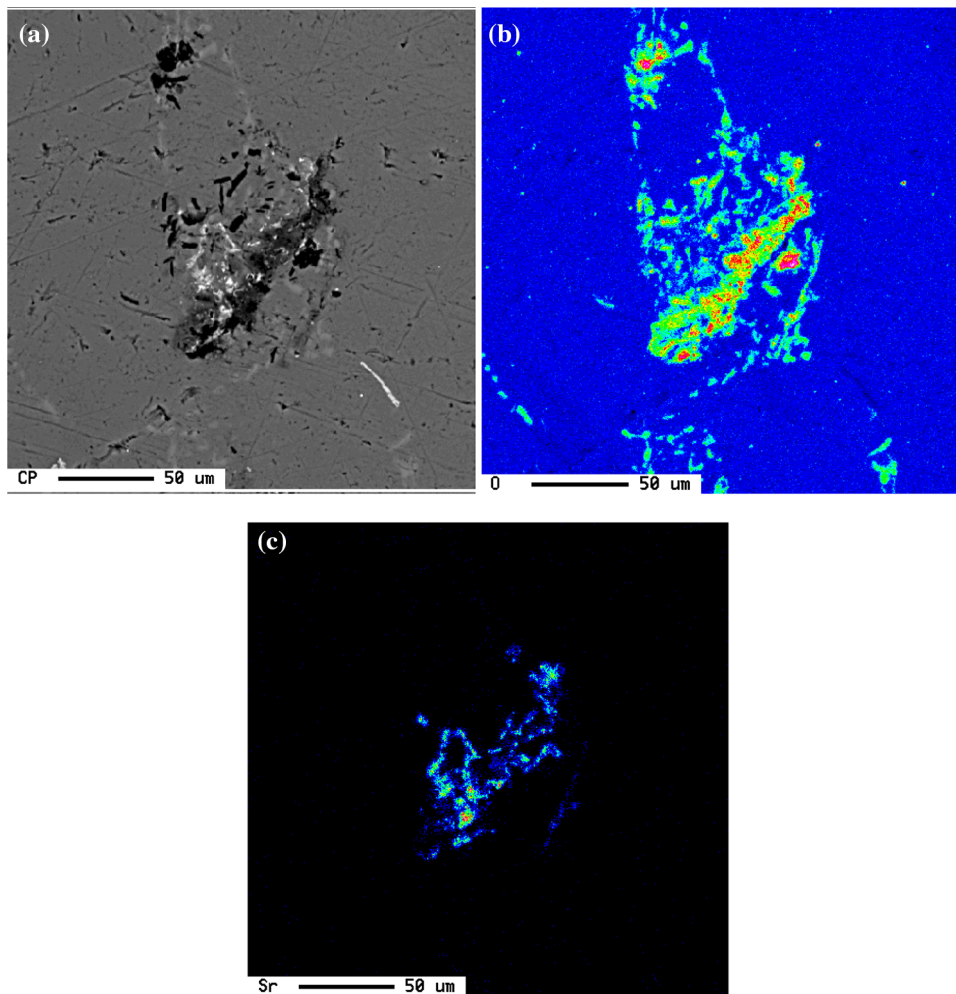


Figure 13. Porosity size and distribution in: (a) DBLS, (b) D3LS, (c) D6LS, (d) D9LS alloy samples.



**Figure 14.** Example of SrO observed inside a pore in D9LS sample-reduced pressure test: (a) backscattered electron image, and corresponding X-ray images of (b) O, and (c) Sr distribution.

### Acknowledgements

The authors would like to thank Amal Samuel for enhancing the quality of the images and figures used in the present article.

### REFERENCES

1. S. Nallusamy, A review on the effects of casting quality, microstructure and mechanical properties of cast Al-Si-0.3 Mg alloy. *Int. J. Perform. Eng.* **12**, 143–154 (2016)
2. R.S. Rana, R. Purohit, S. Das, Reviews on the influences of alloying elements on the microstructure and mechanical properties of aluminium alloys and aluminium alloy composites. *Int. J. Sci. Res. Publ.* **2**(6), 01–07 (2012)
3. A.M. Samuel, H.W. Doty, S. Valtierra, F.H. Samuel, Effect of grain refining and Sr-modification interactions on the impact toughness of Al-Si-Mg cast alloys. *Mater. Des.* **56**, 264–273 (2014)
4. Yu. Chen, Ye Pan, Lu Tao, Shiwen Tao, Wu Jili, Effects of combinative addition of lanthanum and boron on grain refinement of Al-Si casting alloys. *Mater. Des.* **64**, 423–426 (2014)
5. A. Prasada Rao, K.K. Das, B.S. Murty, M. Chakraborty, Microstructural and wear behaviour of hypoeutectic Al-Si alloy (LM25) grain refined and modified with Al-Ti-C-Sr master alloy. *J. Wear* **261**, 133–139 (2006)
6. A.M. Samuel, H.W. Doty, S. Valtierra, F.H. Samuel, Relationship between tensile and impact properties in Al-Si-Cu-Mg cast alloys and their fracture mechanisms. *Mater. Des.* **53**, 938–946 (2014)
7. E. Samuel, B. Golbahar, A.M. Samuel, H.W. Doty, S. Valtierra, F.H. Samuel, Effect of grain refiner on the tensile and impact properties of Al-Si-Mg cast alloy. *Mater. Des.* **56**, 468–479 (2014)

8. D.H. Xiao, J.N. Wang, D.Y. Ding, H.L. Yang, Effect of rare earth Ce addition on the microstructure and mechanical properties of an Al-Cu-Mg-Ag alloy. *J. Alloys Compd.* **352**, 84–88 (2003)
9. Z. Li, X.P. Ling, F. Life, F.F. Guo, Z. Li, X.M. Zhang, Effect of Y on microstructure and mechanical properties of 2519 aluminum alloy [J]. *Trans. Nonferr. Met. Soc. China* **17**, 1191–1198 (2007)
10. D.H. Xiao, B.Y. Huang, Effect of Yb addition on precipitation and microstructure of Al–Cu–Mg–Ag alloys. *Trans. Nonferr. Met. Soc. China* **17**, 1181–1185 (2007)
11. H.C. Fang, K.H. Chen, Z. Zhang, C.J. Zhu, Effect of Yb addition on microstructures and properties of 7A60 aluminum alloy. *Trans. Nonferr. Met. Soc. China* **18**, 28–32 (2008)
12. K.H. Chen, H.C. Fang, Z. Zhang, X. Chen, G. Liu, Effect of Yb, Cr and Zr additions on recrystallization and corrosion resistance of Al-Zn-Mg-Cu alloys. *J. Mater. Sci. Eng. A* **497**, 426–431 (2008)
13. H.C. Fang, K.H. Chen, Z. Zhang, C.J. Zhu, Investigate the effect of Yb additions on microstructures and properties of 7A60 aluminum alloy. *Trans. Nonferr. Met. Soc. China* **18**, 28–32 (2008)
14. G.K. Sigworth, The modification of Al–Si casting alloys: important practical and theoretical aspects. *Int. J. Metalcast.* **2**, 19–40 (2008)
15. A.K. Dahle, J. Taylor, D.A. Graham, The role of eutectic growth mode in porosity formation in Al–Si alloys. *Alum. Trans.* **3**, 17–30 (2000)
16. A. Knuutinen, K. Nogita, S.D. McDonald, A.K. Dahle, Porosity formation in aluminium alloy A356 modified with Ba, Ca, Y and Yb. *J. Light Met.* **1**, 241–249 (2001)
17. D. Ferdian, J. Lacaze, I. Lizarralde, A. Niklas, A. Isabel, F. Ana, Study of the effect of cooling rate on eutectic modification in A356 aluminium alloys. *Mater. Sci. Forum* **765**, 130–134 (2013)
18. S. Hegde, K.N. Prabhu, Modification of eutectic silicon in Al–Si alloys. *J. Mater. Sci.* **43**, 3009–3027 (2008)
19. M. Farkašová, E. Tillová, M. Chalupová, Modification of Al-Si-Cu cast alloy. *FME Trans.* **41**, 210–215 (2013)
20. K. Nogita, S.D. McDonald, A.K. Dahle, Eutectic modification of Al–Si alloys with rare earth metals. *Mater. Trans.* **45**, 323–326 (2004)
21. A.K. Dahle, K. Nogita, S.D. McDonald, C. Dinnis, L. Luc, Eutectic modification and microstructure development in Al–Si Alloys. *Mater. Sci. Eng. A* **413–414**, 243–248 (2005)
22. R. Ahmad, M.B.A. Asmael, Influence of lanthanum on solidification, microstructure, and mechanical properties of eutectic Al–Si piston alloy. *J. Mater. Eng. Perform.* (2016). doi:[10.1007/s11665-016-2139-8](https://doi.org/10.1007/s11665-016-2139-8)
23. S. Samavedam, S. Sundarajan, Al–Si and Al–Si–Mg cast alloys shrinkage porosity estimation. *Arch. Foundry Eng.* **1**, 61–68 (2016)
24. D. Kaka, L. Kovaevi, P. Terek, D. Krumes, Z. Kolumbi, use of sem and eds analysis in the investigation of Al–Si–Cu piston alloy cast porosity. *Metallurgija* **48**, 171–174 (2009)
25. A.M. Samuel, F.H. Samuel, C. Villeneuve, H.W. Doty, S. Valtierra, Effect of trace elements on beta-Al<sub>5</sub>FeSi characteristics, porosity and tensile properties of Al–Si–Cu (319) cast alloys. *Int. J. Cast Met. Res.* **14**, 97–120 (2001)
26. A. Pennors, A.M. Samuel, F.H. Samuel, H.W. Doty, Precipitation of beta-Al<sub>5</sub>FeSi iron intermetallic in Al-6% Si-3.5% Cu (319) type alloys: Role of Sr and P. *AFS Trans.* **106**, 251–264 (1998)
27. A.M. Samuel, H.W. Doty, S. Valtierra, F.H. Samuel, Influence of oxides on porosity formation in Sr-treated alloys. *Int. J. Metalcast.* (2016). doi:[10.1007/s40962-016-0118-3](https://doi.org/10.1007/s40962-016-0118-3)
28. Z. Ma, A.M. Samuel, F.H. Samuel, H.W. Doty, S. Valtierra, A study of tensile properties in Al-Si-Cu and Al-Si-Mg alloys: effect of β-iron intermetallics and porosity. *Mater. Sci. Eng. A* **490**(1–2), 36–51 (2008)
29. H. Liu, A.M. Samuel, F.H. Samuel, H.W. Doty, S. Valtierra, role of strontium oxide on porosity formation in Al–Si casting alloys in Transactions of the American Foundry Society, vol. 110, pp. 449–462; 106th Metalcasting Congress, American Foundry Society, 4–7 May 2002
30. W. Khalifa, F.H. Samuel, J.E. Gruzleski, Iron intermetallic phases in the Al corner of the Al–Si–Fe system. *Metall. Mater. Trans. A* **34**, 807–825 (2003)
31. A.M. Samuel, H.W. Doty, S. Valtierra, F.H. Samuel, Porosity formation in Al–Si sand mold castings. *Int. J. Metalcast.* (2017). doi:[10.1007/s40962-016-0129-0](https://doi.org/10.1007/s40962-016-0129-0)